# Electromagnetic Structure of the Proton and Neutron*

R. HOFSTADTER, F. BUMILLER, AND M. R. YEARIAN

*Department of Physics and High-Energy Physics Laboratory, Stanford University, Stanford, California*

## I. INTRODUCTION

OVER the past few years high-energy electron-scattering measurements have demonstrated clearly the existence of deviations from point-nucleon scattering laws.[1] For the proton, represented by a point charge and a point magnetic moment, the scattering law is given by a formula due to Rosenbluth.[2] At large angles and high energies, deviations between the observed scattering and that given by the point Rosenbluth formula exceed a factor of ten. Recent work has shown that large deviations from point scattering also occur in the case of the neutron.[3–6] The results obtained in the proton and neutron investigations have been interpreted as evidence of the finite sizes of the nucleons.[1,7–9]

In the first part of this paper we try to summarize the results already established, as well as some of the most recent findings of the electron-scattering method. In the second part, we present a brief account of the significance of the observed deviations from point-nucleon scattering.

## II. REVIEW OF EXPERIMENTAL FINDINGS

We take the point of view that the deviations from point scattering may be attributed entirely to finite structure effects in the nucleons. Although it is possible that some part of the deviations can be assigned to a breakdown of electrodynamics at small distances,[7–9] the phenomenological description of the results which we give is not influenced by a choice of either of these alternative explanations, and in many respects the two interpretations are presently indistinguishable. For convenience we adopt the language of finite size effects and return to this fundamental question later in the review.

By a "point" we mean any structure contained entirely within a sphere, whose radius is less than or equal to one nucleon Compton wavelength $=2.1\times10^{-14}$ cm.

### A. Proton

The first observations (Fig. 1) of a finite size of the proton were made by Hofstadter and McAllister.[7,10] Experimental points at the larger angles lie about a factor 1.6 below the theoretical Rosenbluth scattering law for a point proton. These results are not due to instrumental effects as was shown by examining the scattering at 100 Mev, at which energy the finite size effects were expected to play only a small role. At 100 Mev it was indeed found that the angular scattering distribution follows the Rosenbluth law quite satisfactorily,[10] as shown in Fig. 2.

In both Fig. 1 and Fig. 2 the Mott curve is exhibited.

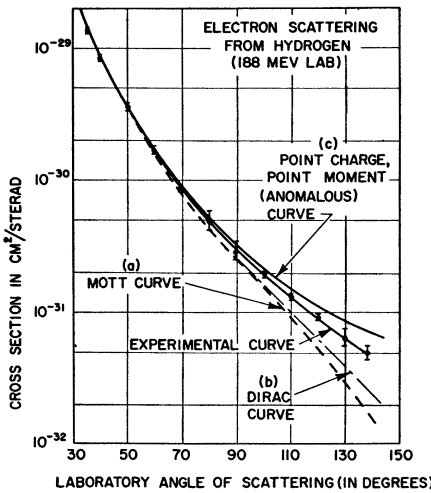


FIG. 1. The Mott curve corresponding to Eq. (1) is labeled (*a*). The Dirac curve (*b*) is given by the Rosenbluth formula, Eq. (2), with $\kappa=0$. Curve (*c*), the "Rosenbluth" curve, is obtained from Eq. (2) with $\kappa=1.79$ and takes into account the full effect of the proton's anomalous magnetic moment. If the proton could be represented by a point charge and a point magnetic moment, curve (*c*) would give the appropriate angular behavior. The experimental points lie below the curve (*c*) and therefore show that the proton has a spread-out structure.

* Supported jointly by the Office of Naval Research, U. S. Atomic Energy Commission, and U. S. Air Force, through the Office of Scientific Research of the Air Research and Development Command.

[1] R. Hofstadter, Ann. Rev. Nuclear Sci. **7**, 231 (1957). This article provides a recent review of electron scattering by nucleons and nuclei.

[2] M. N. Rosenbluth, Phys. Rev. **79**, 615 (1950).

[3] Blankenbecler, Hofstadter, and Yearian. This work was reported in a review article by R. Hofstadter, Revs. Modern Phys. **28**, 214 (1956).

[4] M. R. Yearian and R. Hofstadter, reference 1, pp. 267–271. (See also Proceedings of Seventh Annual Rochester Conference, 1957.)

[5] M. R. Yearian and R. Hofstadter, Bull. Am. Phys. Soc. Ser. II, **2**, 389 (1957).

[6] M. R. Yearian and R. Hofstadter, Phys. Rev. **110**, 552 (1958).

[7] R. Hofstadter and R. W. McAllister, Phys. Rev. **98**, 217 (1955).

[8] Yennie, Lévy, and Ravenhall, Revs. Modern Phys. **29**, 144 (1957).

[9] R. Hofstadter, Revs. Modern Phys. **28**, 214 (1956).

[10] R. W. McAllister and R. Hofstadter, Phys. Rev. **102**, 851 (1956).

The Mott distribution is given by the scattering law

$$\left(\frac{d\sigma}{d\Omega}\right)_{\text{Mott}}=\left(\frac{e^2}{2E_0}\right)^2\frac{\cos^2\theta/2}{\sin^4\theta/2}\times\frac{1}{1+(2E_0/Mc^2)\sin^2\theta/2}=\sigma_{NS} \quad (1)$$

and is abbreviated by the symbol $\sigma_{NS}$. Thus, $\theta$ is the laboratory angle of scattering, and $E_0$ is the laboratory energy of the incident electron. $M$ is the mass of the proton. Mott scattering is expected for a point proton with a charge $(+e)$ but without a magnetic moment. In the derivation of Eq. (1) the *electron* is assumed to have its usual charge and magnetic moment.[1] The presence of the proton's magnetic moment accounts for the additional scattering of a real proton over and above the Mott scattering for a point charge. The fact that the experimental curve (Fig. 1) lies between the Mott curve and the Rosenbluth point-charge, point-magnetic moment curve is taken as the evidence of finite structure in the proton. The ratio of the experimental scattering cross section to the Rosenbluth point-scattering cross section is called the square of the "form factor."[1,9]

The Rosenbluth point scattering curve is

$$\left(\frac{d\sigma}{d\Omega}\right)=\sigma_{NS}\left\{1+\frac{\hbar^2q^2}{4M^2c^2}[2(1+\kappa)^2\tan^2\theta/2+\kappa^2]\right\}, \quad (2)$$

where

$$q=-\frac{2}{\lambda}\frac{\sin\theta/2}{[1+(2E_0/Mc^2)\sin^2\theta/2]^{\frac{1}{2}}}=\frac{2E_0}{\hbar c}\frac{\sin\theta/2}{[1+(2E_0/Mc^2)\sin^2\theta/2]^{\frac{1}{2}}}. \quad (3)$$

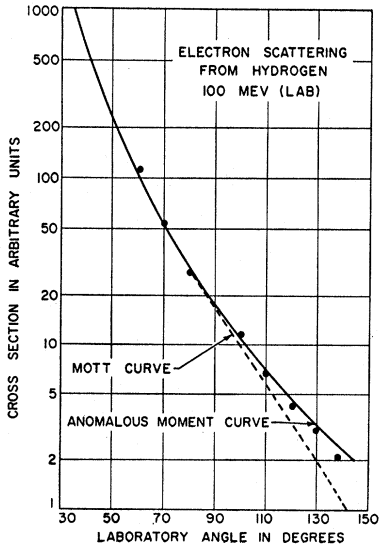


FIG. 2. At 100 Mev the effects of finite size are small and the experimental points, shown as black dots, lie very close to the point Rosenbluth curve, the upper of the two theoretical curves drawn in the figure.

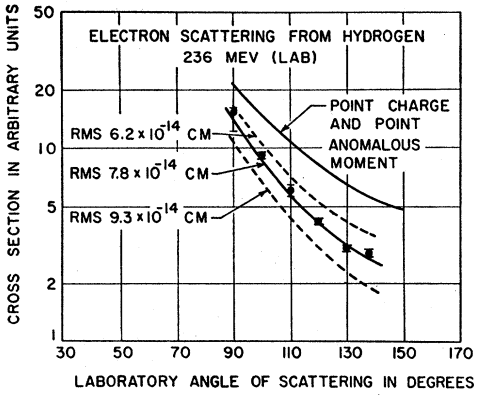


FIG. 3. Experimental points taken at an incident electron energy of 236 Mev are shown. The point-charge, point-moment curve is shown for comparison along with theoretical curves allowing for finite size effects. An rms of $0.78\times10^{-13}$ cm gives good agreement with the experimental data. The best-fitting curve was chosen on the basis of relative cross sections rather than on absolute cross-section values. The choice $0.78\times10^{-13}$ cm is in good agreement with the data in Figs. 1 and 2.

Here, $\kappa(=1.79)$ is associated with the Pauli or anomalous part of the proton's magnetic moment, and $q$ is the so-called electron's (four-vector) energy-momentum-transfer.[1] Rosenbluth[2] and others[1,8,11] have shown that finite size effects or equivalently phenomenological form factors can be introduced into Eq. (2) as follows:

$$\left(\frac{d\sigma}{d\Omega}\right)=\sigma_{NS}\left\{F_1^2+\frac{\hbar^2q^2}{4M^2c^2}[2(F_1+\kappa F_2)^2\times\tan^2\theta/2+\kappa^2F_2^2]\right\}. \quad (4)$$

$F_1$ and $F_2$ are the phenomenological form factors and are individually functions of the invariant momentum-transfer $q$. $F_1$ is associated with the Dirac charge and intrinsic magnetic moment of the proton and $F_2$ is associated with the Pauli part of the moment $(\kappa)$. $F_2$ is usually associated with the mesonic cloud making up the outer parts of the proton's electromagnetic structure, and, in principle, can be obtained from a meson field theory. Early attempts to calculate the form factors $F_1$, $F_2$ were made by Rosenbluth[2] on the basis of a weak-coupling theory.

Further experiments on the proton were carried out by McAllister and Hofstadter[10] at an electron energy of 236 Mev. Their results are shown in Fig. 3. The figure indicates that an rms radius of the proton equal to $(0.78\pm0.20)\times10^{-13}$ cm provides a good fit with the experimental data. This "size" was in good agreement with the radius $(0.70\pm0.24)\times10^{-13}$ cm obtained in the 188-Mev experiment.[7]

The numerical results were arrived at by assuming that

$$F_1=F_2(\equiv F_P) \quad (5)$$

[11] For important contributions to the development of Eq. (4), see reference 8 and the references therein.

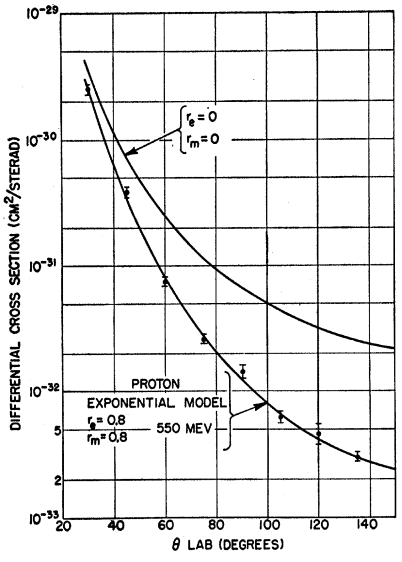


FIG. 4. The experimental electron-proton-scattering data of Chambers and Hofstadter[12] observed at an incident energy of 550 Mev. The Rosenbluth point-charge curve is shown above. Drawn through the experimental points is a theoretical curve with $F_1=F_2$ and a choice of an exponential model of the proton, Eq. (8), with appropriate choices of the rms radii. The best fit is obtained with $r_e=r_m=0.80\times10^{-13}$ cm.

as functions of $q$ and effectively using the shape-independent approximation.

$$F=1-(q^2a^2/6)+\cdots, \tag{6}$$

where "$a$" is the rms radius of the charge or magnetic moment distribution. Equation (6) can be used where the higher terms in the expansion can be neglected, as in the case of the early data. $F$ is related more generally to a density distribution through the Fourier transform[1,8,9]

$$F=\frac{4\pi}{q}\int_0^\infty \rho(\mathbf{r})\exp(i\mathbf{q}\cdot\mathbf{r})d^3\mathbf{r}, \tag{7}$$

which applies in the nonrelativistic limit in which $\rho(\mathbf{r})$ is the static density distribution and is a function of radius. When only small values of $qa$ are involved, the expression (7) can be replaced by Eq. (6) and a size (rms radius) determined. In the experiments reported here, it is not practical to use Eq. (6), because many higher terms are involved in the expansion, i.e., it is possible to determine more than one parameter from the experiments. It would, of course, be desirable to determine "$a$" carefully in the shape-independent approximation, but since the deviations from point scattering are then small, the experiments require high accuracy and are difficult to perform.

The assumption, Eq. (5), that $F_1=F_2$ is an arbitrary one. However, the early experiments were in very good agreement with this assignment. Subsequent events have proved that $F_1=F_2$ in the current range of momentum transfers is a surprisingly good approximation. At large angles, where $\tan\theta/2\gtrsim1$, and at high energies, it becomes possible to distinguish magnetic moment scattering from charge scattering. Hence it becomes possible to find $F_1$ and $F_2$ separately.

Using a new magnetic spectrometer, Chambers and Hofstadter[12] carried out a detailed series of experiments on the proton extending to an energy of 550 Mev with scattering angles lying between 30° and 135° in the laboratory frame. These experiments showed at once very large deviations from point scattering. Typical data are reproduced in Fig. 4 and show the large reduction from point scattering (upper curve) due to finite size effects. Drawn through the experimental points is a

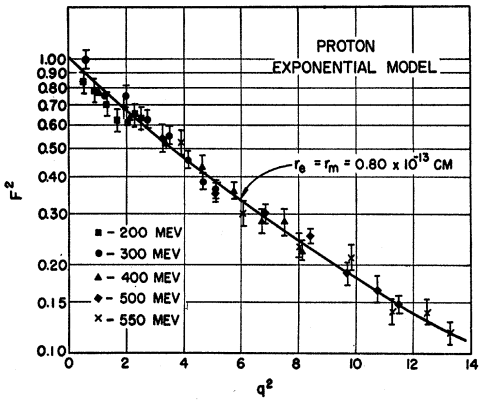


FIG. 5. $F_P^2(F_P=F_1=F_2)$ is plotted against $q^2$ in units of $10^{+26}$ cm$^{-2}$. The solid line represents the $F_P^2$ curve for an exponential model of a proton with $r_e=r_m=0.80\times10^{-13}$ cm. The experimental points are those of Chambers and Hofstadter.[12] The fitting procedure is described in the text.

theoretical curve calculated with Eq. (4) for $F_1=F_2=F_P$, where $F_P$ corresponds by Eq. (7) to the transform of a charge density (and magnetic moment density) belonging to the exponential family

$$\rho=\rho_0\exp(-12^{\frac{1}{2}}r/a), \tag{8}$$

and thus $F_P$ is

$$F_P(qa)=\frac{1}{[1+(q^2a^2/12)]^2}. \tag{9}$$

The fit is quite good. The agreement with experiment is excellent at all other energies as well. However, an equally good fit with experiment could be made with a Gaussian charge density (and Gaussian magnetic moment density) which leads also to a Gaussian form factor. Over the range of $q$ values studied in these experiments, the exponential model, with rms radius $0.80\times10^{-13}$ cm of the charge cloud ($F_1$), and rms radius $0.80\times10^{-13}$ cm of the magnetic moment cloud, was indistinguishable from Gaussian density distributions, when a required change was made in the rms radii. For Gaussians the rms radii were very close to $0.70\times10^{-13}$ cm. Figures 5 and 6 show the two corresponding graphs

[12] E. E. Chambers and R. Hofstadter, Phys. Rev. **103**, 1454 (1956).

of $F^2$ *versus* $q^2$ for the two models. The fitting procedure used in preparing Figs. 4–6 was based on the shape of the angular distributions and not on absolute values of the cross sections. Although absolute cross sections were obtained by Chambers and Hofstadter, they were not sufficiently accurate to distinguish between such models. Therefore, in fitting data at various energies, slight adjustments of the $F^2$ ratios were made by sliding the entire experimental distribution at a given energy up and down until the best match between theory and experiment was obtained. The just-discernible variations in $F^2$ between Figs. 5 and 6 represent the effects of such shifts. It also proved possible, with $F_1=F_2$, to find other one-parameter models which could fit the data. Such models are shown in Fig. 7, where $4\pi r^2\rho$ is plotted against radius. A model (Yukawa I) which does not fit is also shown. A uniform charge distribution cannot be made to fit the data.

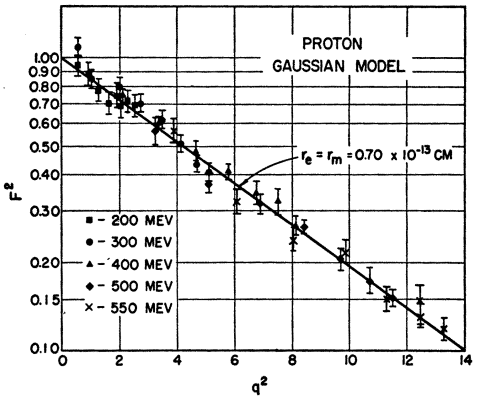


FIG. 6. This figure is similar to Fig. 5 except that a Gaussian model of the proton is employed to calculate $F_P^2$. On the basis of the data in Figs. 5 and 6, either the exponential or Gaussian model is satisfactory. Higher energies are needed to decide between these two models (see following).

When $F_1=F_2$, it is possible to plot a single curve showing $F^2$ at all energies. When $F_1\neq F_2$ this is not possible, and a separate curve must be prepared for each energy. Figure 8, from Chambers and Hofstadter, shows an attempt to satisfy the experimental data with a model in which the $F_1$ corresponds to a point ($r_e=0$), and the $F_2$ is adjusted to give the best fit obtainable under these conditions with a Gaussian model ($r_m=1.0\times10^{-13}$ cm). No shifting of the theoretical curves will permit a fit with the data. Other simple models for $F_2$ with $r_e=0$ were also tried without success. It was concluded that a point charge and spread-out magnetic moment would not yield agreement with the experimental results. Small magnetic radii were also unsuitable, as shown by a typical choice reproduced in Fig. 9. Chambers[13] considered many combinations of different

[13] E. E. Chambers, "Electron-proton scattering at electron energies up to 550 Mev," Ph.D. thesis, Stanford University (May, 1956).

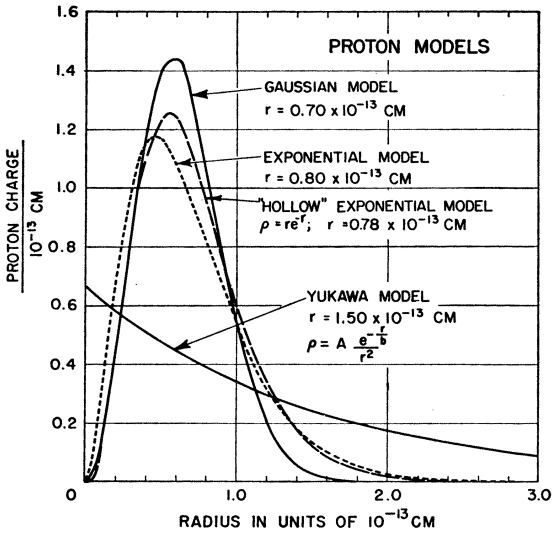


FIG. 7. This figure shows a plot of $4\pi r^2\rho$ *versus* radial distance from the center of the proton. Three models are shown (Gaussian, exponential, and hollow exponential) which fit the Chambers-Hofstadter experiments. $4\pi r^2\rho$ is a quantity proportional to the amount of charge in a shell at radius $r$. The Yukawa distribution, also shown in the figure, cannot be made to fit the data with any choice of radius. For these models, $F_1$ is taken equal to $F_2$.

choices for $F_1$ and $F_2$, i.e., $F_1\neq F_2$, and concluded that within certain experimental errors no choice would fit the data as well as $F_1=F_2$, for the successful models discussed above (and reproduced in Fig. 7). In Fig. 7 values of $4\pi r^2\rho$ are plotted in preference to $\rho$ itself, because the experiments are presently not sensitive to values of $\rho$ at small radii. The plot in Fig. 7 deemphasizes the density at small radii and is more useful.

The ratio, $F_1/F_2$, may be found independently of any model by comparing two cross sections at two different energies and two different angles, such that the momen-

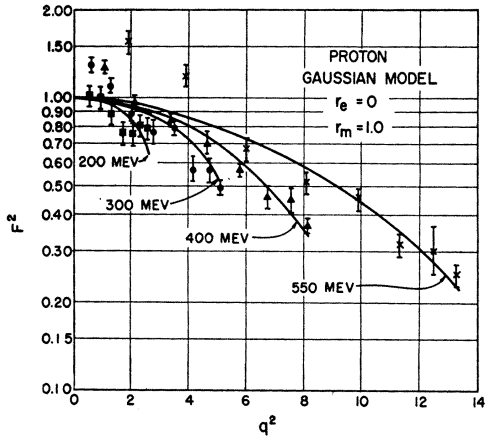


FIG. 8. This figure shows an attempt to fit the Chambers-Hofstadter results, at all the energies used in the experiments, with a Gaussian model such that $r_e=0$ and $r_m$ is chosen to give the best agreement with experiment. $r_m=1.0\times10^{-13}$ cm for this case. The fit is not satisfactory and this model can be excluded. With $F_1\neq F_2$, as in this case, separate theoretical curves are required for the various values of incident energy.

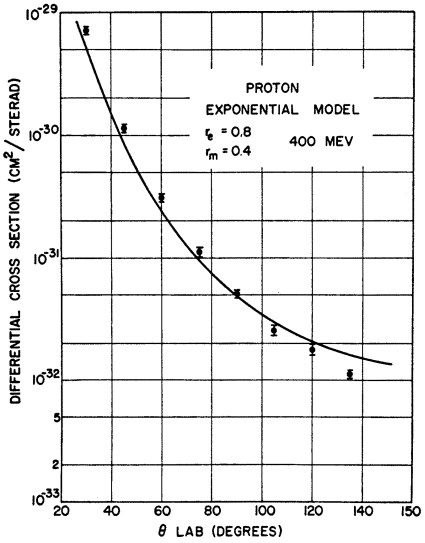


FIG. 9. A small magnetic radius of the proton cannot be made to satisfy the experimental data at 400 Mev. Similar results hold at other energies. The experimental points are those of Chambers and Hofstadter.[12]

tum transfer $q$ is the same at both cross section determinations. At $q^2 \cong 4\times10^{26}$ cm$^{-2}$, a value of $F_1/F_2 = 1.1\pm0.2$ was found from the experiments.[12] At $q^2 = 9.33\times10^{26}$ cm$^{-2}$, $F_1/F_2 = 1.04\pm0.2$.[14]

Using the fact that magnetic moment scattering falls off more slowly at large angles than charge scattering, the large-angle, high-energy data may be analyzed to find $F_1+\kappa F_2$. Since $\kappa = 1.79$, the data can yield $F_2$, if $F_1$ is known even approximately. Now, when $F_2$ becomes known approximately, e.g., by the method outlined above, the situation may be turned about by studying the small-angle data as a function of energy. At small angles the magnetic scattering is essentially zero, and hence $F_1$ may be investigated alone, that is, the scattering is practically purely charge scattering. Although $F_2$ enters into the cross-section calculations at small angles, the magnetic scattering (involving $F_2$) is small, so that even large errors in determining $F_2$ will not affect the results for $F_1$. Thus, by a series of successive steps first at small angles and then at large angles, $F_1$ and $F_2$ may be determined separately.

These procedures are demonstrated in Fig. 10, where

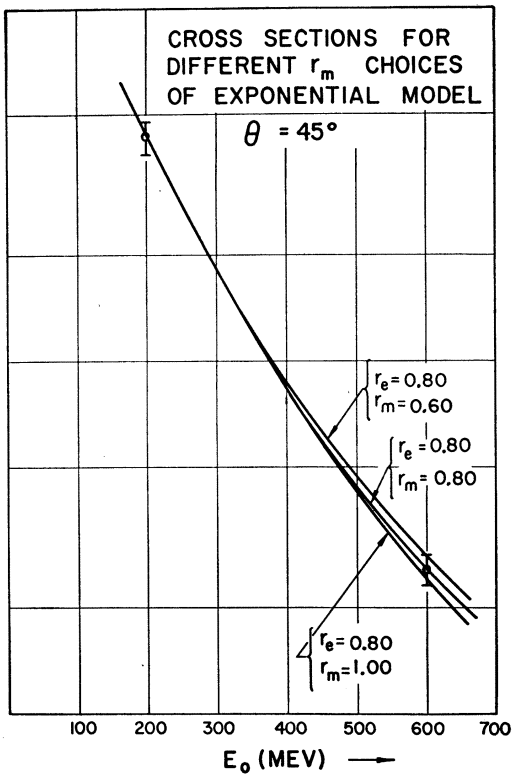


FIG. 10. This figure shows that a relatively large uncertainty in the value of $F_2$ (or in the choice of magnetic radius) has very little influence on the small-angle electron-proton cross sections as a function of energy. The experimental points represent the recent data of Bumiller and Hofstadter.[14]

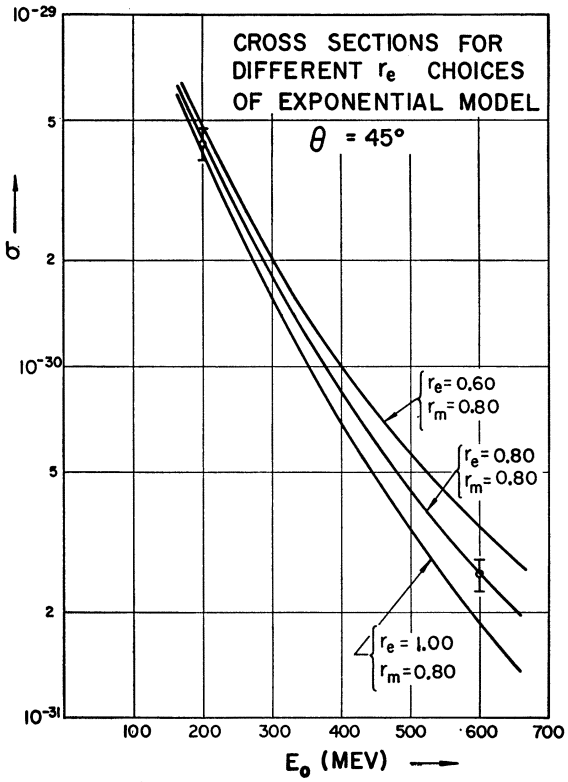


FIG. 11. This figure shows that the small-angle data (45°) are sensitive to the choice of $F_1$ (or the choice of electrical radius). Recent experimental data of Bumiller and Hofstadter,[14] shown in the figure, support the choice of $r_e = r_m = 0.80\times10^{-13}$ cm and an exponential model of the proton.

[14] F. Bumiller and R. Hofstadter (to be published).

the small influence on $F_1$ of a relatively large uncertainty in $F_2$ is shown. In this figure the magnetic rms radius is allowed to vary, for an exponential model, from $r_m=0.60\times10^{-13}$ cm to $r_m=1.0\times10^{-13}$ cm, while the cross section at 45° is shown as a function of $E_0$. The large changes in $r_m$ barely produce an error as large as the experimental uncertainty. On the other hand, the recent 45° data,[14] shown in Figs. 10 and 11, show that, for an exponential model, the charge rms radius must be close to $0.80\times10^{-13}$ cm. This result agrees very well with the earlier conclusions of Chambers and Hofstadter.

From this presentation it has become clear that one need not talk of models. It is sufficient to find $F_1$ and $F_2$ separately, as already indicated. We have used the model approach simply because it provides a convenient mnemonic device for calculating the $F$'s under all conditions of scattering. If preferred the reader may use the Fourier transform [Eq. (9)] without ever thinking of the model. In this way, however, he loses sight of the spatial spreading of the density functions, which is especially of interest in connection with the charge densities of light nuclei, where the proton's spatial extent definitely contributes to the spreading of the nuclear charge throughout the nuclear volume and surface. While we may speak of a model, we wish it to be understood that we really mean that the Fourier transform of this model provides phenomenological form factors fitting the experimental data.

The value $r_e=0.80\times10^{-13}$ cm has been confirmed by McAllister,[15] who measured an absolute cross section for electrons of 189.6 Mev scattering from protons at 60° and found a value of $(1.20\pm0.07)\times10^{-30}$ cm²/sterad. In this shape-independent determination, McAllister found a radius of $0.75\times10^{-13}$ cm consistent with the more accurate determination $(0.80\pm0.04)\times10^{-13}$ cm discussed above.[14]

An independent analysis of the elastic scattering of electrons by the deuteron has been carried out by McIntyre[16] and by McIntyre and Dhar.[17] In these experiments the magnetic effects are very small and the charge scattering appears essentially by itself. If it is assumed that the *neutron charge density* distribution does not influence the scattering of electrons by deuterons, which appears to be a very reasonable assumption from the experiments on the neutron-electron interaction,[18–23] the charge size of the proton is determined and is consistent with the rms size $0.80\times10^{-13}$ cm. In fact, the experiment may be turned about[17] and used to determine the neutron-proton potential in the deuteron. At present, however, the deuteron elastic data are not sufficiently accurate to decide between various commonly used potentials.

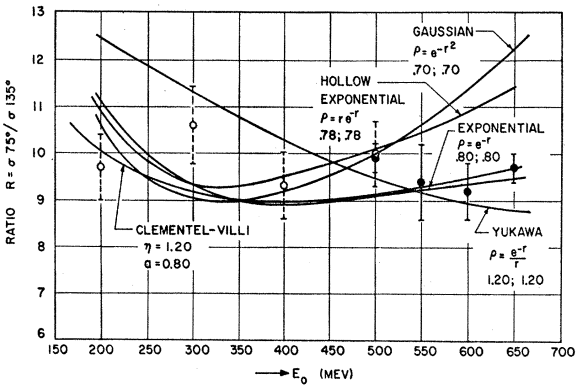


FIG. 12. The ratio of electron-proton cross sections at 75° and 135° is plotted as a function of incident energy. This type of measurement does not require a knowledge of absolute cross sections. The data of Bumiller and Hofstadter[14] are shown as solid circles while earlier data of Chambers and Hofstadter[12] are shown as hollow circles. The new data eliminate a Gaussian model with $r_e=r_m=0.70\times10^{-13}$ cm. The hollow exponential model ($r_e=r_m=0.78\times10^{-13}$ cm) is also excluded. The Yukawa model is excluded by this figure as well as other data (not shown in the figure). The exponential model with radii $0.80\times10^{-13}$ cm still provides a satisfactory fit with all the experiments.

Recent extension of the proton data by Bumiller and Hofstadter[14] now makes it possible to distinguish between the various models proposed by Chambers and Hofstadter.[12] Figure 12 shows the behavior of the ratio $R$

$$R=\left(\frac{d\sigma}{d\Omega}\right)_{75°}\Big/\left(\frac{d\sigma}{d\Omega}\right)_{135°} \tag{10}$$

as a function of the incident energy for electron scattering from the proton. The experimental ratio is found to be almost constant and lies between 9.0 and 10.0 from 200 to 650 Mev. The dashed experimental points (hollow circles) show some of the Chambers-Hofstadter results and do not distinguish between the models (except for the Yukawa case, which provides a poor fit at small angles). The new data in Fig. 12 (solid points) now serve to distinguish between the various models and show that, for $F_1=F_2$, the exponential model with rms radii, $r_e=0.80\times10^{-13}$ cm and $r_m=0.80\times10^{-13}$ cm, fits the data very well. As explained above this should be understood to mean that Eq. (9) is to be used as the appropriate phenomenological form factor. Its square is given in Fig. 13 and extends to larger $q^2$ values than the older data.

A systematic attempt to study values of the total $F^2$ for $F_1\neq F_2$ and two different models is illustrated in Figs. 14 and 15. At 600 Mev and 45° the choices $r_e$, $r_m$, shown in the third column, are made for form factors of the type given by Eq. (9). The values of the total (form

[15] R. W. McAllister, Phys. Rev. **104**, 1494 (1956).
[16] J. A. McIntyre, Phys. Rev. **103**, 1464 (1956).
[17] J. A. McIntyre and S. Dhar, Phys. Rev. **106**, 1074 (1957).
[18] E. Fermi and L. Marshall, Phys. Rev. **72**, 1139 (1947); Hamermesh, Ringo, and Wattenberg, Phys. Rev. **85**, 483 (1952).
[19] Havens, Rainwater, and Rabi, Phys. Rev. **82**, 345 (1951).
[20] D. J. Hughes and M. T. Burgy, Phys. Rev. **81**, 498 (1951); Ringo, Hughes, and Burgy, Phys. Rev. **84**, 1160 (1951).
[21] Hughes, Harvey, Goldberg, and Stafne, Phys. Rev. **90**, 497 (1953); Melkonian, Rustad, and Havens, Bull. Am. Phys. Soc. Ser. II, **1**, 62 (1956).
[22] B. T. Feld, *Experimental Nuclear Physics*, edited by E. Segré (John Wiley and Sons, Inc., New York, 1953), Vol. II, p. 208. This article gives a summary of the experiments. See also Crouch, Krohn, and Ringo, Phys. Rev. **102**, 1321 (1956).
[23] See also reference 8 for a discussion of neutron size.

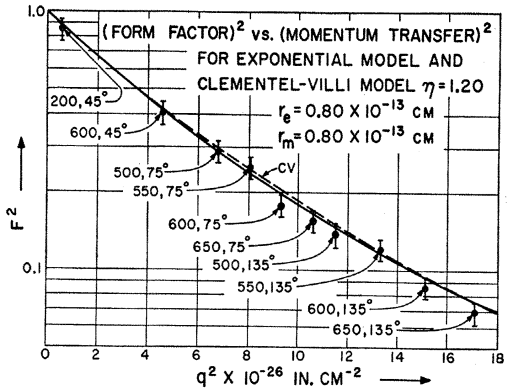


FIG. 13. The value of $F_P^2(F_1=F_2=F_P)$ is shown as ordinate in this figure and the abscissa is $q^2$ in appropriate units. This curve is similar to the one shown in Fig. 5 but is here extended to larger values of $q^2$ by the new experiments of Bumiller and Hofstadter.[14] Two equivalent choices of model are made: the exponential model and the Clementel-Villi model. The Clementel-Villi model is described in the text [Eqs. (11) to (13)]. The present experiments do not distinguish between these models.

factor)², i.e., the ratio of the calculated cross section to the point cross section, are shown in the fourth column. The absolute experimental value is shown in the fifth column in bold numerals with values permitted by experimental error in light numerals. The choices in the third column in bold numerals are permitted. The other choices are eliminated. Similar calculations are made for a Gaussian form factor, shown in the sixth column. The bars through the bold numerals mean that these possible choices have been eliminated, because such choices do not fit the experimental data at other angles and energies (see Fig. 15, 650 Mev, 135°). Thus no Gaussian will do.

In Fig. 15 a similar table shows that the Gaussian is unsatisfactory. The table also shows that only the form factor, corresponding to $r_e=0.80\times10^{-13}$ cm, $r_m=0.80\times10^{-13}$ cm for an exponential model, Eq. (9), is satisfactory, within, of course, the present experimental error.

Such studies do not preclude the possibility of finding other models which fit the data. In spite of the fact that

| $E_0$ MEV | $\theta$ | $r_e$ | $r_m$ | TOTAL $F^2$ EXPONENTIAL | EXPERIMENTAL ± 10 % | GAUSSIAN |
|---|---|---|---|---|---|---|
| | | | | | | |
| | | 0.6 | 0.6 | .597 | | .570 |
| | | **0.8** | **0.6** | **.448** | | ~~.408~~ |
| | | 1.0 | 0.6 | .336 | | .208 |
| | | | | | | |
| | | 0.6 | 0.8 | .562 | .450 | .530 |
| 600 | 45° | **0.8** | **0.8** | **.411** | **.410** | ~~.372~~ |
| | | 1.0 | 0.8 | .302 | .370 | .243 |
| | | | | | | |
| | | 0.6 | 1.0 | .534 | | .500 |
| | | **0.8** | **1.0** | **.386** | | .340 |
| | | 1.0 | 1.0 | .276 | | .220 |

FIG. 14. The chart shows, by example, how different proton models may be distinguished between by the experimental data at 600 Mev and 45° (5th column). Descriptions of the method and the various columns in the figure are given in the text.

many models have been examined, it is still possible that one with a singularity at the origin will satisfy the experiments. It is probable, however, that this can occur only if the singularity contains a small fraction of the total charge. If the region about the singularity contains a large fraction of the protonic charge, we believe it unlikely that a model fitting the data could have been missed.

As an example of the above remarks, we consider a model having some theoretical justification. This model has been proposed by Clementel and Villi.[24] For this model (abbreviated C-V)

$$\rho(\mathbf{r})=\frac{\eta k^2}{4\pi r}\exp(-kr)-(\eta-1)\delta(\mathbf{r}), \tag{11}$$

where $-(\eta-1)\delta(\mathbf{r})$ represents a negative singularity (a negative point charge) at the origin and $(\eta-1)$ determines the numerical fractional amount of proton charge placed in the singularity. The spread-out part of the C-V model is a Yukawa II distribution with $\eta$-total

| $E_0$ MEV | $\theta$ | $r_e$ | $r_m$ | TOTAL $F^2$ EXPONENTIAL | EXPERIMENTAL ± 10 % | GAUSSIAN |
|---|---|---|---|---|---|---|
| | | | | | | |
| | | 0.6 | 0.6 | .194 | | .146 |
| | | 0.8 | 0.6 | .143 | | .096 |
| | | 1.0 | 0.6 | .116 | | ~~.072~~ |
| | | | | | | |
| | | 0.6 | 0.8 | .115 | .080 | ~~.071~~ |
| 650 | 135° | **0.8** | **0.8** | **.076** | **.070** | .036 |
| | | 1.0 | 0.8 | .056 | .060 | .022 |
| | | | | | | |
| | | 0.6 | 1.0 | ~~.076~~ | | .040 |
| | | 0.8 | 1.0 | .045 | | .015 |
| | | 1.0 | 1.0 | .029 | | .006 |

FIG. 15. This figure is similar to Fig. 14 except that the experimental data refer to 650 Mev and 135°. An explanation of the table will be found in the text.

proton charges and has a low order positive singularity at the origin. The model provides a form factor

$$F(q)=\frac{1+\left(\frac{1-\eta}{k^2}\right)q^2}{1+q^2/k^2}, \tag{12}$$

and the rms radius is found to be

$$a=(1/k)(6\eta)^{\frac{1}{2}}. \tag{13}$$

As mentioned above, the C-V model may be considered a physical way of citing the form factor expression Eq. (12). Calculations with the C-V model (subject to $F_1=F_2$) show that an excellent fit with all the data, extending between 100 Mev and 650 Mev, is obtained with $\eta=1.2$ and $a=0.80\times10^{-13}$ cm. The theoretical C-V curve is shown in Fig. 13 as a dashed line. Thus a negative point charge with 20% of the value of the

[24] E. Clementel and C. Villi, Nuovo cimento 4, 1207 (1956).

proton charge can be placed at the center of the physical proton, and a positive spread-out charge amounting to 1.2 proton charges can be distributed around the negative point center as a Yukawa II cloud. The form factors, corresponding to this C-V distribution and to an exponential model with rms radius $0.80\times10^{-13}$ cm are indistinguishable within experimental error, as far as a value of $q^2=17$, which is as far as the present experiments go. Since the C-V ($\eta=1.2$, $a=0.80\times10^{-13}$ cm) $F$'s resemble closely the $F$'s for an exponential model ($a=0.80\times10^{-13}$ cm), the $F_1$ may be chosen to belong to one model and an $F_2$ to the other. Within experimental error $F_2$ may also be selected from other closely fitting models, without prejudice.

It is not claimed that an actual proton resembles the C-V model, but this example demonstrates that *non-*

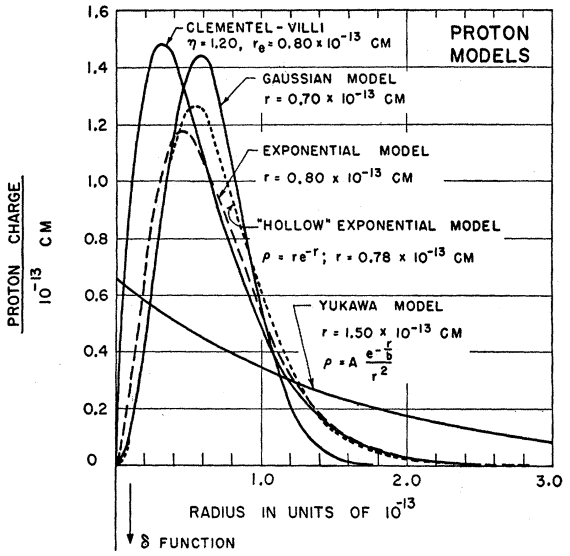


FIG. 16. A plot ($4\pi r^2\rho$) similar to Fig. 7 is shown. However, this figure shows also the Clementel-Villi model which fits the experimental data quite well (see Fig. 13). In the C-V model a negative $\delta$ function and a positive Yukawa II distribution are used and the density function is not monotonic. The C-V model fits best with $\eta=1.20$ and $a=0.80\times10^{-13}$ cm (see text).

*monotonic* density distributions can be made to represent the experimental data. In such cases the $4\pi r^2\rho$ distributions, similar to those shown in Fig. 7, will be nearly the same outside a certain small volume near the center of the proton. For example, Fig. 16 compares the C-V ($\eta=1.2$) and exponential models with $F_1=F_2$ and $r_e=r_m=0.80\times10^{-13}$ cm for each of the models. Outside a radius $0.4\times10^{-13}$ cm, the C-V and exponential models have essentially the same $4\pi\rho r^2$ behavior. In Fig. 13 the C-V values of $F^2$ are plotted and are essentially indistinguishable from those of the exponential model. The significance of this example is that the present experiments probe the outside of the proton and are noncommittal about details in the central ($r\leqslant0.4\times10^{-13}$ cm) parts of that structure. However, it is unlikely that a monotonic type of singularity exists in the center of the proton containing more than a small fraction of the proton's charge.

This material describes the information accumulated up to the present concerning the proton's structure. The interpretation has been carried out using the Rosenbluth formula, Eq. (4), including the phenomenological form factors $F_1$ and $F_2$. Drell and Ruderman[25] and Drell and Fubini[26] have shown that the Rosenbluth representation, including $F_1$ and $F_2$, should be accurate within a few percent up to energies approaching 1.0 Bev, even at large angles.

### B. Neutron

Experiments on the neutron[27] were motivated by a desire to see whether the small neutron size (essentially zero), found in experiments on the neutron-electron interaction,[18–23] implies as well a small rms radius of the magnetic moment cloud in the neutron. Early ideas[27] indicated that a study of the inelastic breakup of the deuteron by energetic electrons might provide an excellent way of probing the magnetic structure in the neutron. Thus a nucleon scattering electrons with high momentum-transfer ($q$) and at a large angle ($\tan\theta/2\gg1$), does so by virtue of its magnetic moment. That the "charge" scattering is small under these conditions is shown by the Rosenbluth equations (2) or (4). Hence proton scattering should not exhibit a much greater cross section than neutron scattering, if both nucleons possess approximately the same magnetic moment structure. The only reason that a proton should scatter with a greater cross section than a neutron is traceable, for the extreme conditions described in the foregoing, to the large numerical value of its magnetic moment ($\mu_P=2.79$ nm; $\mu_N=-1.91$ nm). Equation (4) for a proton and Eq. (14), for a free neutron, derived from Eq. (4)

$$\left(\frac{d\sigma}{d\Omega}\right)_N=\sigma_{NS}F_{2N}{}^2\kappa_N{}^2\frac{\hbar^2q^2}{4M^2c^2}[2\tan^2\theta/2+1], \quad (14)$$

by placing $eF_1{}^N\cong0$ (static charge and second moment for the neutron are both zero), show that the scattering cross section is proportional to the square of the nucleon's magnetic moment. In thus comparing the scattering by a free neutron and a free proton, the neutron-proton ratio would be approximately $(1.91)^2/(2.79)^2=0.45$, if the nucleons should have similar magnetic structures. If the neutron should have a point magnetic moment while the proton is spread out, the ratio at 500 Mev and 135° would be 3.0 instead of 0.45! This follows, because the proton's (form factor)$^2$ results in a reduction of the proton cross section to approximately 0.15 times the point cross section at 500 Mev and 135°. A deviation

[25] S. Drell and M. Ruderman, Phys. Rev. **106**, 561 (1957).
[26] S. Drell and S. Fubini (to be published).
[27] R. Hofstadter, Revs. Modern Phys. **28**, 214 (1956). See Sec. VI of this article for the early work on the neutron size by electron-scattering methods.

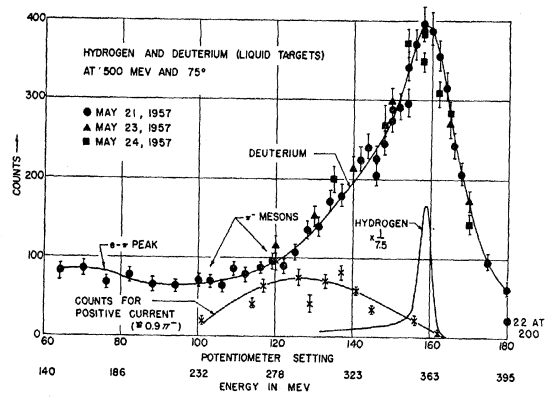


FIG. 17. The inelastic peak corresponding to scattering of 500 Mev electrons from deuterons at an angle of 75° in the laboratory system. Note the wide spread of scattered electron's energies compared with the sharp electron-proton peak near 360 Mev. The experimental data are those of Yearian and Hofstadter.[6] The deuteron curve should be multiplied by 0.87 to allow for the different densities of liquid deuterium and liquid hydrogen. The data are immediately seen to be incompatible with a neutron whose magnetic moment is a point.

from 0.45 as large as 3.0 can easily be detected. The goal of our neutron experiment is suggested to be the determination of which (if either) of the two above values corresponds to nature.

Unfortunately, free neutrons cannot be obtained in sufficient numbers to carry out electron-scattering experiments. The deuteron, however, offers an excellent vehicle for the test, since it is basically a weakly bound structure, having a low binding energy ($\epsilon = 2.23$ Mev). Moreover, the conditions needed to make the simple ratio measurement, i.e., large momentum transfer, etc., are just those required to make the scattering from the neutron and proton in the deuteron essentially independent of the binding. The deuteron breakup (=incoherent scattering) at large $q$ thus provides a fortunate possibility to study the neutron's magnetic structure.

It is possible that an extraordinarily large fourth moment in the neutron's *charge* distribution could contribute to the scattering cross section, but this seems extremely unlikely.

The fact that the nucleons are bound in the deuteron does imply that the incoherent scattering peak, observed at a given angle from the deuteron, will not have the sharp appearance characteristic of the proton peak.

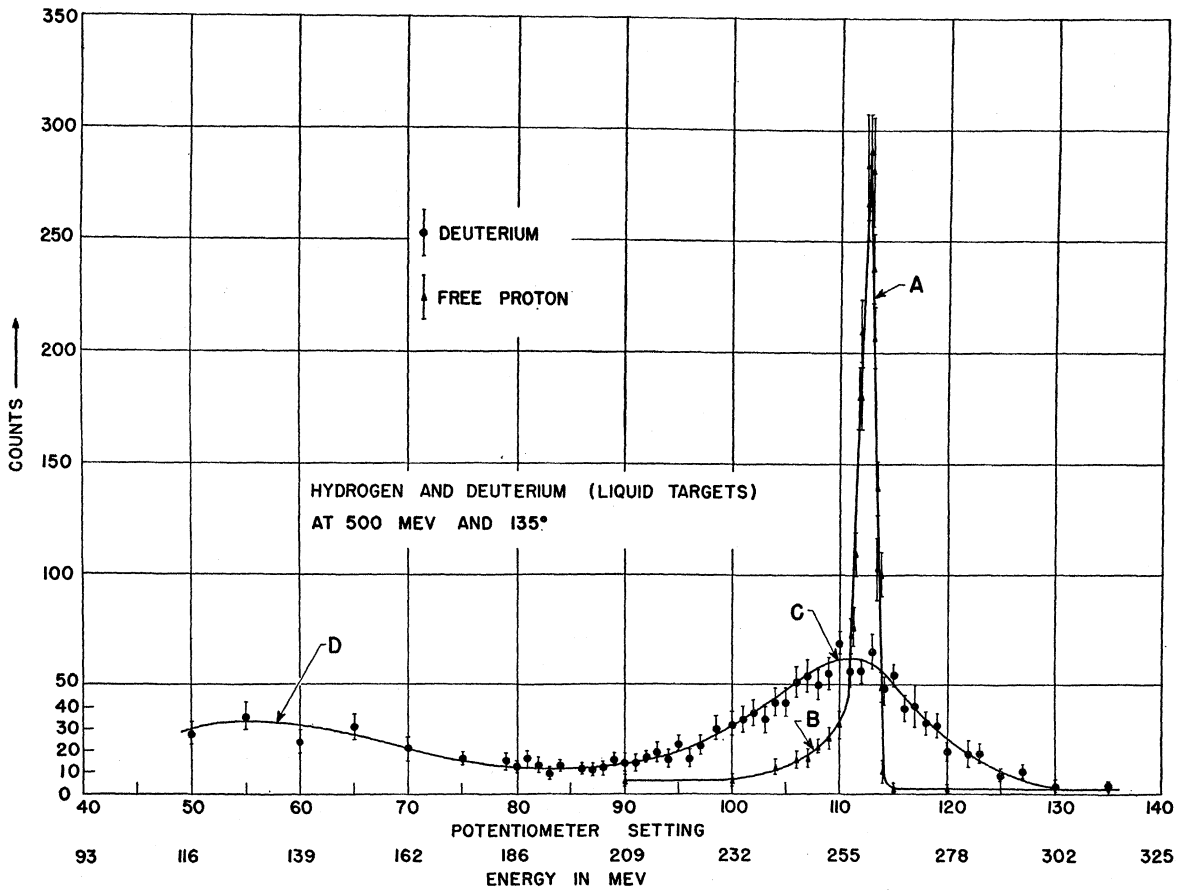


FIG. 18. Data of Yearian and Hofstadter[6] showing electron-deuteron inelastic scattering at an incident electron energy of 500 Mev and a scattering angle of 135°. The corresponding sharp proton peak is also shown. The deuteron curve should be multiplied by 0.87 as in Fig. 17. From such curves the neutron's electron-scattering cross section can be obtained. The neutron's cross section is too small to correspond to a point magnetic moment.

Instead, the deuteron peak will be spread out over a momentum (or for electrons, energy) range, given by the internal momentum distribution of the nucleons moving within the deuteron. Such an inelastic peak was observed early in the electron-scattering experiments.[28] Recent data[5,6,29] of the same kind are illustrated in Figs. 17, 18, and 19. They show that the areas under the deuteron peaks are too small to give a ratio $(d\sigma/d\Omega)_N/(d\sigma/d\Omega)_P=3.0$. Thus, the neutron's magnetic structure is not a point! In fact, the deuteron areas contain scattering due to the bound proton, and when this cross section is allowed for by subtraction, the residual neutron cross section is comparable with and smaller than that of the free proton.

In the present consideration we have been using implicitly the idea described in Eq. (15), where

$$\left(\frac{d\sigma}{d\Omega}\right)_D=\left(\frac{d\sigma}{d\Omega}\right)_P+\left(\frac{d\sigma}{d\Omega}\right)_N, \qquad (15)$$

and where $(d\sigma/d\Omega)_D$, $(d\sigma/d\Omega)_P$ are abbreviations for the integrated areas in Figs. 17, 18, and 19 under the deuteron and proton curves, respectively. The ordinates in these figures are differential cross sections with respect to angle and energy, thus $(d^2\sigma/d\Omega dE)_D$, $(d^2\sigma/d\Omega dE)_P$, etc. The neutron cross section of Eq. (15) can be obtained as a difference between the deuteron and proton cross sections (~areas in above figures). (In making the comparison, the deuteron curves should be multiplied by 0.87 to allow for the different densities of liquid deuterium and liquid hydrogen.) An equation such as (15) cannot be valid exactly, but Jankus[30] and Blankenbecler[31] have shown that it is remarkably good. Blankenbecler has used a closure rule to obtain this result. Jankus' results are described below.

The corrections needed to make an equation of type (15) valid appear to be of the order of a few percent. Although the corrections are small, they are important. Fortunately, it is not necessary to depend on knowing these corrections, because a second (and probably better) method for finding neutron size makes use of the *peak* of the deuteron curve instead of the area. Nevertheless, since the "area method" was used at first and since it provides a crude model-independent approximation to the correct answer, we describe briefly the consequences of comparing the deuteron area with the proton area.

Equation (15) may be replaced, in first approximation, by Eq. (16) where $\Delta$ represents the effect of the small corrections described above.

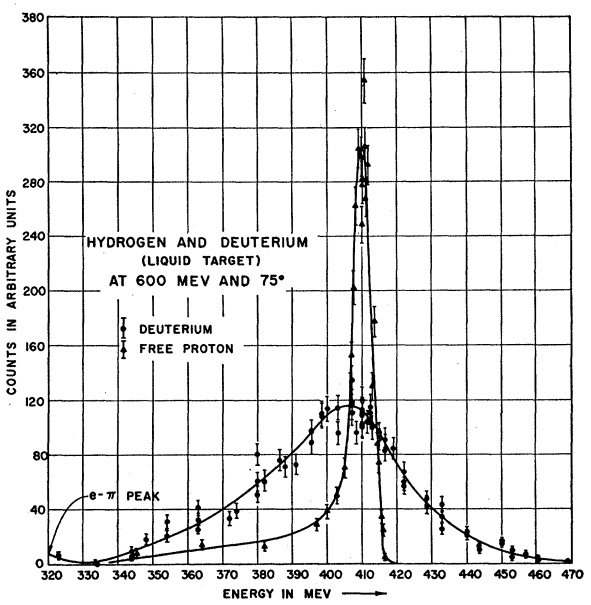


FIG. 19. The inelastic electron-deuteron scattering peak observed at the highest energy (600 Mev) at which such experiments have been carried out. The deuteron curve should be multiplied by 0.87 as in Fig. 17. The data are those of Yearian and Hofstadter[29] and were obtained at a scattering angle of 75° in the laboratory system. The comparison electron-proton peak is also shown in the figure. A point magnetic moment in the neutron would give a larger deuteron scattering peak.

$$\left(\frac{d\sigma}{d\Omega}\right)_D=(1+\Delta)\left\{\left(\frac{d\sigma}{d\Omega}\right)_P+\left(\frac{d\sigma}{d\Omega}\right)_N\right\}. \qquad (16)$$

The two terms in the final bracket of Eq. (16) are given by Eqs. (4) and (14), respectively. Thus, $\Delta$ will include kinematic effects resulting from motion of the nucleons and also the influence of variations in form factors of the finite nucleons over the momentum spread in the deuteron. Furthermore, $\Delta$ will include an effect corresponding to interaction of the two nucleons in the final state. These corrections have been discussed in detail by Blankenbecler[31] and also more briefly in references 1 and 6. However, the size of the correction $\Delta$ is indicated by the following examples: At 500 Mev and 75°, $\Delta\cong 0.004$ and at 500 Mev and 135°, $\Delta\cong 0.03$. Thus the corrections are very small.

One additional contribution to $\Delta$, difficult to calculate, concerns a meson exchange effect, in which, for example, a meson created on one of the nucleons by the electron is reabsorbed by the second nucleon, after which the electron flies off. Such meson exchange effects may contribute to $\Delta$ an additional amount, of the order of 10%.[32] This correction is discussed in references 1 and 6. Some information may be found empirically about meson exchange effects, by comparing the low-energy side of the experimental deuteron peaks

[28] J. A. McIntrye and R. Hofstadter, Phys. Rev. **98**, 158 (1955).
[29] M. R. Yearian and R. Hofstadter, Bull. Am. Phys. Soc. Ser. II, **3**, 50 (1958).
[30] V. Z. Jankus, Phys. Rev. **102**, 1586 (1956).
[31] R. Blankenbecler, Bull. Am. Phys. Soc. Ser. II, **2**, 389 (1957). See also reference 1 of this article where Blankenbecler's work is reported.
[32] S. Drell and R. Blankenbecler (private communication).

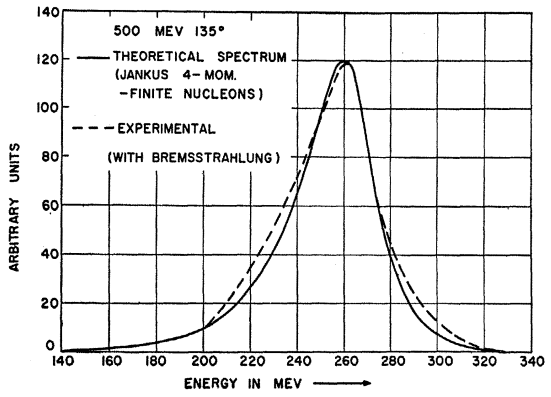


FIG. 20. The solid line is the result of a theoretical calculation, using the modified Jankus theory (see text), for the inelastic continuum corresponding to electron scattering from the deuteron at an angle of 135° at an incident electron energy of 500 Mev. The dashed line represents the experimental results. The theoretical curve takes account of bremsstrahlung, the effect of finite nucleon size, and substitution of four-momentum transfer for three-momentum transfer. The curves are normalized at the peaks.

with the shape of the curves predicted by the Jankus theory.[30] Such a comparison is made in Fig. 20 between an experimental and a Jankus theoretical curve. We now show how it is possible to compute the theoretical curves such as the one in Fig. 20. We then return to the area considerations and to the meson exchange effects.

In Fig. 20 the solid line is obtained from Eqs. (9) to (11) of Jankus' paper with suitable modifications: For point nucleons the Jankus formulas [Jankus, Eqs. (9) to (11)] may be used to provide inelastic continua such as the one shown in Fig. 21. Also shown are the corrections to the continuum due to the interaction in the final state. These final state corrections have been mentioned above. Jankus (point) curves, computed from his Eqs. (9) to (11) for the conditions under which the experiments have been performed, have several defects. (1) They do not include the effects of finite sizes of the nucleons. (2) They do not include effects of

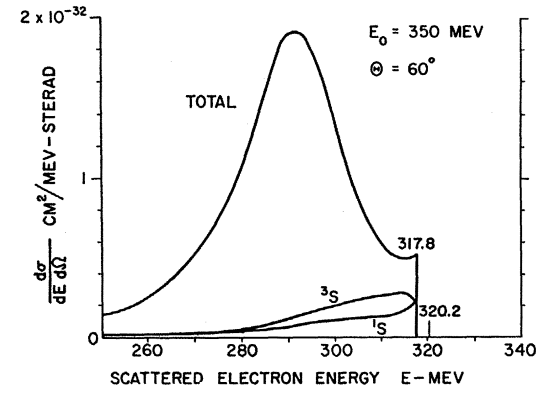


FIG. 21. Electron scattering from the deuteron according to the original Jankus[30] theory for point nucleons. The $^3S$ and $^1S$ interactions in the final state are shown below but are included in the upper curve.

bremsstrahlung, whereas the experiments do. (3) They do not reduce, at high energies, where binding can be neglected, to a sum of Rosenbluth formulas for the two nucleons.

Effect (3) was noticed immediately when the curves were compared with experiment. Each Jankus curve at a given angle showed a peak at an energy slightly different from the position of the experimental peak. At 500 Mev at 75° the Jankus peak appeared at an energy 2% below the experimental peak, and for 500 Mev at 135° the Jankus peak appeared at an energy about 5% below the experimental position. These shifts are not large, but are well outside experimental error (~1%) and indicate a systematic failure of the formulas. To make the Jankus formulas reduce to the Rosenbluth ones at high energy, it was necessary to replace the three-momentum transfer[1] ($s$) in Jankus' work with the four-momentum transfer ($q$). With this correction, all the peaks appeared in the correct experimental positions at all angles and energies. The ordinates of the Jankus

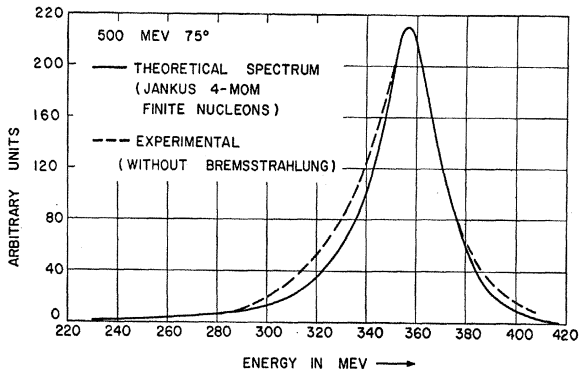


FIG. 22. This figure is similar to Fig. 20 and shows a comparison between the data of Yearian and Hofstadter[6] and the modified Jankus theory.

curves were affected very little, although the widths at half-maxima were modified slightly.[33] This was a very satisfactory step.

Another small change was required, since $\kappa_p^2$ appears in the Rosenbluth formula [last term in Eq. (2)], whereas $\mu_p^2=(1+\kappa_p)^2$ appears in the Jankus formulas. This is a very small term and its modification has little significance.

After the four-momentum was inserted into the Jankus formulas, it became quite easy to incorporate the effects of finite size, because the $F^2$ *vs* $q^2$ curves are known for the proton and could be inserted separately for the neutron. In the trials made so far, $F_{2N}$ has been taken equal to $F_{2P}$. This now appears to be rather definite from additional evidence (peak method, see below). Thus Effects (3) and (1) were taken care of.

Effect (2) was taken into account by folding the shape of the observed proton peak, bremsstrahlung included, into the deuteron inelastic curves of Jankus,

[33] See reference 6 for details.

as modified above. This was a simple, although tedious, operation. Since the deuteron curve is already rather broad (~40 to 45 Mev width at half-maximum), the bremsstrahlung folding operation had little effect on the width.

In this way theoretical curves of the type shown in Fig. 20 were prepared for many angles at the energies 500 and 600 Mev. In all cases tested the experimental and theoretical curves were in unexpectedly good agreement (Figs. 20 and 22). The good agreement was unexpected since meson-exchange effects have not been included in the Jankus calculations. Furthermore, in the calculations performed at these high energies, the interaction in the final state was ignored. This was done without fear since the final state effects are governed by a form factor which rapidly reduces their values at high energy. In addition, experimental observations such as those shown in Fig. 23, at 600 Mev and 60°,

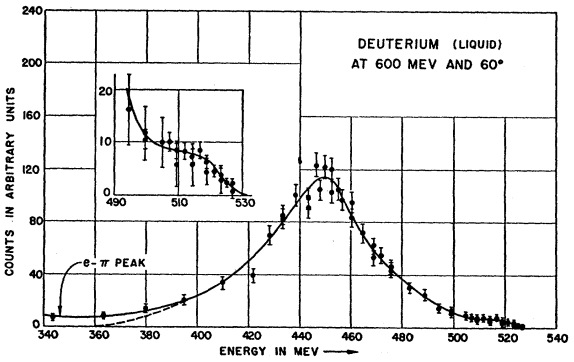


FIG. 23. The experimental inelastic continuum[29] for the deuteron at an energy of 600 Mev and 60°. In the inset and at the right extremum of the inelastic distribution there is a small plateau. This can be shown to be at the correct position and possesses the correct area to be given by the electron-deuteron *elastic* scattering peak. Thus there is very little that can be ascribed to the final-state interactions at this energy and angle.

demonstrate how small the final state interaction effect is under these conditions. When the deuteron elastic peak is allowed for, there is essentially nothing left for final state interaction. At large angles the final state effect is even smaller.

Summarizing the above observations, we may say that a comparison between the modified Jankus theory (modified for four-momentum, finite size, bremsstrahlung) and experiment may now be expected to single out effects not included in the calculations, such as a possible meson exchange contribution to the inelastic scattering. The deviations between the experimental and theoretical curves of Fig. 20 and Fig. 22 may be thought of in this way. Differences in observed shape do not lie far outside the limits of experimental error, so that it can probably be said that experiment now gives evidence of rather small effects of meson exchange in inelastic scattering from the deuteron. Perhaps the deviations on the low-energy side of the inelastic curves

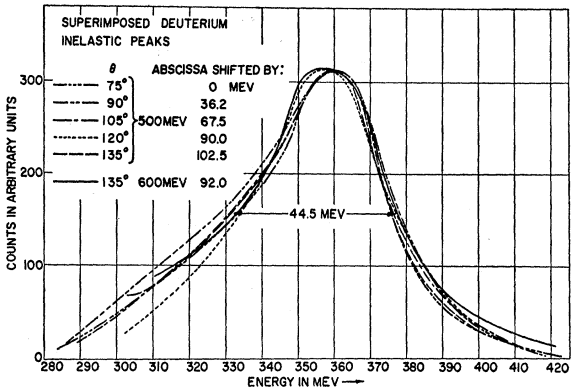


FIG. 24. When the electron-deuteron inelastic peaks are superimposed,[6] they all have approximately the same shape and width at half-maximum. The average width at half-maximum is approximately 45 Mev. This behavior is predicted by the modified Jankus theory and furnishes support for this theory.

of Figs. 20 and 22 are due to meson exchange and those on the right side to small interactions in the final state. Other possible causes of the deviations on both sides of the peak can be due to experimental errors, to inexactness in the Jankus three-momentum→four-momentum conversion, errors in the bremsstrahlung folding, imperfect knowledge of the neutron-form factor (this latter influences the shape only a trifle), etc. On the whole, the fact that the calculated curves agree as well as they do, over so broad a range of energies and angles, must be treated as strong evidence for the modified Jankus theory. Our extension of the Jankus theory appears to be valid beyond the range of energies for

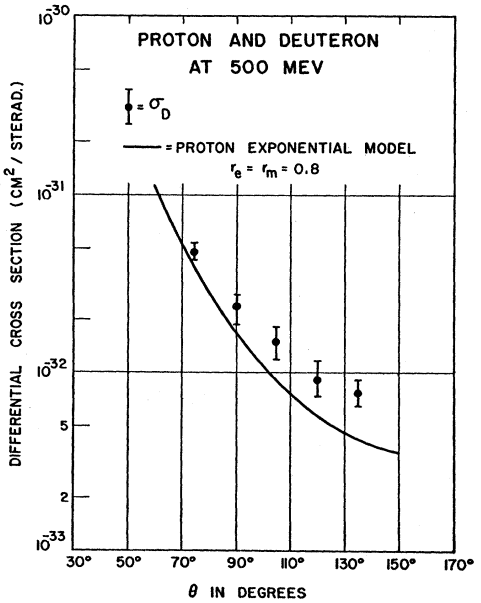


FIG. 25. The total cross sections under the deuteron inelastic continua are plotted as a function of scattering angle at 500 Mev. The comparison electron-proton curve is also shown at 500 Mev. From this curve the ratio $R$ of Eq. (20) may be formed and values of $F_{2N}^2$ may be computed.

which the theory was originally developed. This is true at least approximately after making our modifications.

An additional check on the modified theory is related to the widths of the inelastic continua: Experiment shows that the widths at half-maxima of the deuteron inelastic peaks, observed at various angles and energies, are all essentially constant and approximate 45 Mev. This is shown in Fig. 24 and in Fig. 19. The approximate constancy of the width at half-maximum of the deuteron peaks is a feature of the Jankus theory and is thus further evidence that the modified theory is basically correct, even at such large values of momentum transfer. At very small angles the widths of the inelastic peaks are reduced, also as required by theory.

For the calculations reported here, the Jankus equations (9), (10), and (11) were replaced by

$$d^2\sigma_{in}=\frac{1}{4\pi}\frac{e^4}{p_0^2}\frac{\cos^2\theta/2}{\sin^4\theta/2}\left(\frac{2\alpha}{1-\alpha r_t}\right)\frac{1}{q^2k}O^2d\Omega_p dp, \quad (17)$$

where:

$$O^2=\left\{\frac{1}{Z^2-1}+\frac{1}{Z_1^2-1}-\frac{2}{Z_1-Z}[Q_0(Z)-Q_0(Z_1)]\right\}\left\{F_{1P}^2+\left[F_{1P}^2k^2+2\left(\frac{q}{2}\right)^2(F_{1P}+\kappa_P F_{2P})^2\right.\right.$$

$$\left.+2\left(\frac{q}{2}\right)^2\kappa_N^2F_{2N}^2\right]\tfrac{1}{2}[2\tan^2\theta/2+1-Z^2k^2]-\left(\frac{q}{2}\right)^2(F_{1P}^2+2F_{1P}F_{2P}\kappa_P)\Big\}$$

$$-\left\{\frac{Z}{Z^2-1}+\frac{Z_1}{Z_1^2-1}-\frac{Z_1+Z}{Z_1-Z}[Q_0(Z)-Q_0(Z_1)]\right\}2Zk^2F_{1P}^2-\left\{2+\frac{1}{Z^2-1}+\frac{1}{Z_1^2-1}-\frac{2ZZ_1}{Z_1-Z}[Q_0(Z)-Q_0(Z_1)]\right\}$$

$$\times\left\{\tfrac{1}{2}[2\tan^2\theta/2+1-Z^2k^2]-Z^2k^2\right\}k^2F_{1P}^2-\frac{(Z_1-Z)^2}{ZZ_1(Z_1+Z)}[Q_0(Z)+Q_0(Z_1)][-\tfrac{2}{3}(F_{1P}+\kappa_P F_{2P})\kappa_N F_{2N}]$$

$$\times\left(\frac{q}{2}\right)[2\tan^2\theta/2+1-Z^2k^2], \quad (18)$$

and where

$$\left.\begin{aligned}Z&=\frac{\Delta E}{qk}=\frac{\alpha^2+k^2+q^2/4}{qk}\\ Z_1&=\frac{\gamma^2+k^2+q^2/4}{qk}\\ Q_0(Z)&=\operatorname{arc\,coth}Z=\tfrac{1}{2}\ln\left(\frac{Z+1}{Z-1}\right).\end{aligned}\right\} \quad (19)$$

Here, $p_0$ is the incoming electron momentum, and $p$ is the outgoing (scattered) electron momentum. The vector $\mathbf{k}$ is the final momentum of the proton with respect to the center of mass of the recoiling deuteron.

TABLE I. Total cross sections for the deuteron at 500 and 600 Mev at various scattering angles.

| 500 Mev | | 600 Mev | |
|---|---|---|---|
| $\theta$ | $d\sigma_D/d\Omega$ (cm²/sterad) | $\theta$ | $d\sigma_D/d\Omega$ (cm²/sterad) |
| 45° | ... | 45° | $(2.84\pm0.29)\times10^{-31}$ |
| 60° | ... | 60° | $(7.63\pm0.77)\times10^{-32}$ |
| 75° | $(4.60\pm0.49)\times10^{-32}$ | 75° | $(3.31\pm0.34)\times10^{-32}$ |
| 90° | $(2.36\pm0.40)\times10^{-32}$ | 90° | $(1.08\pm0.19)\times10^{-32}$ |
| 105° | $(1.50\pm0.30)\times10^{-32}$ | 105° | $(9.58\pm2.40)\times10^{-33}$ |
| 120° | $(9.06\pm1.98)\times10^{-33}$ | 120° | $(4.79\pm1.15)\times10^{-33}$ |
| 135° | $(7.58\pm1.23)\times10^{-33}$ | 135° | $(3.09\pm0.60)\times10^{-33}$ and $(2.92\pm0.19)\times10^{-33}$ |

The ground-state wave function of the deuteron is the Hulthén wave function $e^{-\alpha r}-e^{-\gamma r}$, where $\alpha^2$ = binding energy and $\gamma$ is fixed by the choice of the triplet effective range $r_t$.

We used the four-vector energy-momentum transfer for $q$; and for convenience, the formulas are expressed in dimensionless form, i.e., $\hbar=c=M=1$. The $F$'s were put into the appropriate places demanded by the phenomenological theory[11] and by a proper reduction of the result to a sum of Rosenbluth formulas. No attempt was made to insert $F_{1N}$, because it is believed that this quantity lies very close to zero at all of the $q$ values used in these experiments. The Jankus results, appearing in Eqs. (17) to (19) were obtained with a Hulthén potential, and it is not expected that the results will be sensitive to the neutron-proton potential[34] (<5%), although the small corrections corresponding to interaction in the final state may be affected by a choice of potential.

We return to the neutron size determination. To find a first approximation to the neutron size, we may now make a comparison between the deuteron areas under the peaks of Figs. 17, 18, and 19, and the areas under the corresponding proton curves. Typical data[6] taken at 500 Mev, 135°, are shown in Fig. 25 and in Table I along with the proton curve. The ratio $R$ of cross

[34] V. Z. Jankus, "Theoretical aspects of electron-deuteron scattering," Ph.D. thesis, Stanford University (December, 1955).

sections, when $F_{1P}=F_{2P}=F_P$, is easily shown to be

$$R=\left(\frac{d\sigma}{d\Omega}\right)_N\Big/\left(\frac{d\sigma}{d\Omega}\right)_P$$
$$=\frac{F_{2N}^2}{F_P^2}\times\frac{\dfrac{\kappa_N^2\hbar^2q^2}{4M^2c^2}[2\tan^2\theta/2+1]}{1+\dfrac{\hbar^2q^2}{4M^2c^2}[2(1+\kappa_P)^2\tan^2\theta/2+\kappa_P^2]}, \quad (20)$$

and $F_{2N}^2$ may be found from this equation, knowing $F_P$ and $R$. It is desirable to use $R$ in this method, since it is a directly measurable quantity. Using the data of Fig. 25 and more recent data at 600 Mev,[29] an $F_{2N}^2$ *vs* $q^2$ plot for the neutron may be prepared. Such values of $F_{2N}^2$ are shown in Fig. 26. The proton $F^2$ values are also shown in the figure. A (form factor)$^2$ curve for an exponential model with rms radius $r_m=0.80\times10^{-13}$ cm provides a fair fit to the neutron data. The errors are fairly large, but it is clear that the ratio of cross sections is far lower than the value 3.0 (for a point neutron). At the large $q$ values, the ratio is possibly as high as 0.50. The two values, $r_m{}^N=0.8\times10^{-13}$ cm and ratio$=0.50$ are to be compared with the values $r_m{}^P=0.80\times10^{-13}$ cm and ratio$=0.45$, if the neutron and proton had exactly the same structures. Thus our first approximation to the neutron size shows that neutron and proton are very similar. If, e.g., a Gaussian distribution had been used for the neutron, the resulting size would have been a little smaller, but approximate equality of neutron and proton would still hold.

Fortunately, it is possible to improve on the accuracy of the comparison between the neutron and the proton. Drell[35] has pointed out that a determination of the *peak*

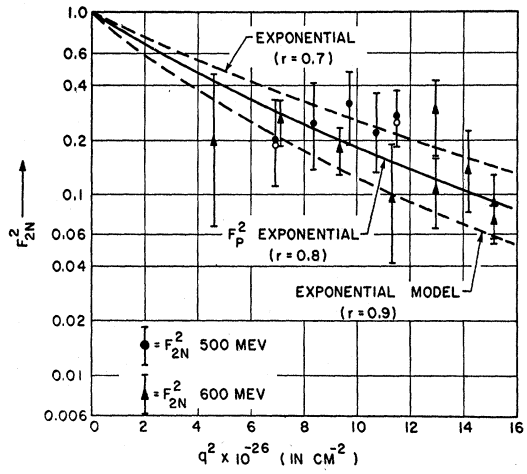


FIG. 26. This figure shows the value of $F_{2N}^2$ for the neutron plotted against $q^2$ for the data taken at 500 and 600 Mev. The dashed curves are theoretical curves given by the exponential model of the magnetic moment density of the neutron. The proton $F_P^2$ is shown as the solid line for comparison.

[35] S. Drell (private communication).

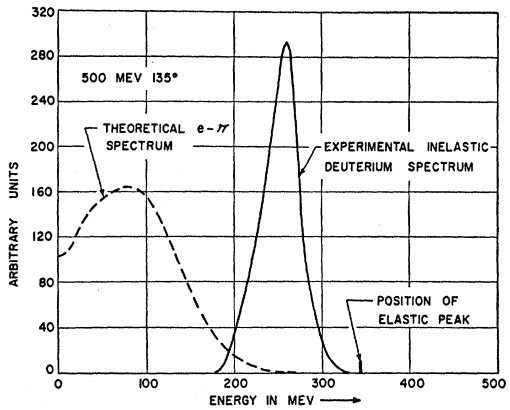


FIG. 27. This figure shows the small overlap between the electron-pion peak and the deuteron's inelastic continuum. The latter is the object of measurement in these studies. At other angles the overlap is smaller. The electron-pion spectrum was calculated from a theory of Dalitz and Yennie into which the deuteron momentum spread was folded.

ordinate of the deuteron inelastic continuum should give a more accurate means of finding the neutron's magnetic structure. This proposal would compare the experimental values of $(d^2\sigma/d\Omega dE)_D$ and the proton area $(d\sigma/d\Omega)$. Since the latter is known from past and recent proton work, the former can be determined by direct observation with considerable accuracy. Furthermore, and this is the main point, the various corrections needed in using the area method (contributants to $\Delta$) are almost all zero at the position of the deuteron's inelastic peak. The interaction in the final state falls to zero in the neighborhood of the peak. The meson-exchange effects fall close to zero at this same position, because there is not enough energy in the center-of-mass system to excite the isobaric state of a nucleon ($\frac{3}{2}$–$\frac{3}{2}$ resonance). Experimentally speaking, the situation is quite favorable also because the deuteron peak and proton peak are always very close to each other, and in a ratio measurement many experimental errors must cancel out. The "contamination" of the deuteron peak by electrons, which have produced real pions, is also negligibly small at the position of the peak. This is shown[6] in the example of Fig. 27, where the theoretical electron-pion section is extremely small at the position of the deuteron peak. For (at least) all the above reasons, the "peak-comparison method" is to be preferred over the "area comparison" method. A possible cause of error in the peak method might exist if the deuteron ordinate at the peak depends on the neutron-proton potential. Recent estimates by Drell and Blankenbecler[36] and Schneider[37] make it seem unlikely that such a variation could exceed 5%. We, therefore, consider the peak method a more reliable index of the neutron's magnetic structure than the area method.

[36] S. Drell and R. Blankenbecler (private communication).
[37] W. Schneider (private communication).

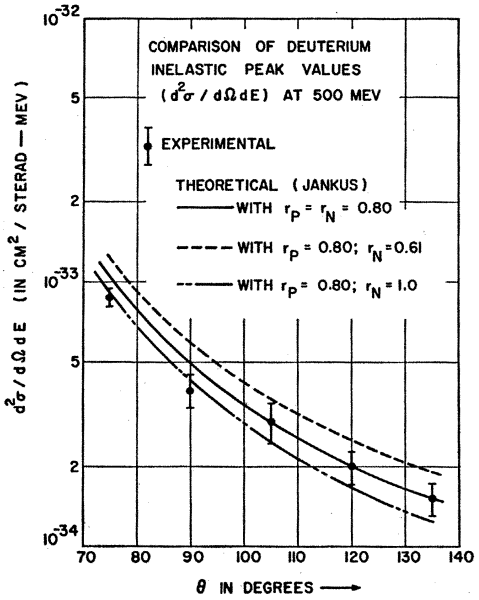


FIG. 28. The maximum values of the deuteron's inelastic cross section are plotted according to the differential cross-section method as a function of scattering angle. The data are those of Yearian and Hofstadter.[6] Theoretical curves have been prepared using the modified Jankus theory. Three such curves are shown. The dashed curves have been prepared for an exponential model of the neutron's magnetic moment density with the indicated rms radii. The solid line represents the same model with an rms radius of $0.80\times10^{-13}$ cm. The proton radii were taken to be $0.80\times10^{-13}$ cm for the exponential model. The experimental points fall slightly nearer the $0.80\times10^{-13}$ curve.

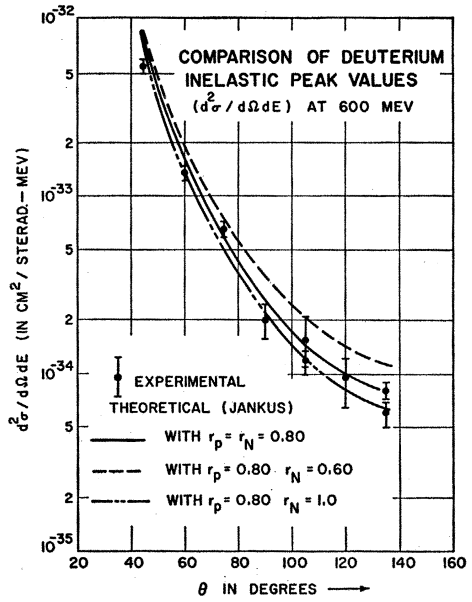


FIG. 29. This figure is similar to Fig. 28 except that the experimental data, due to Yearian and Hofstadter,[29] refer to 600 Mev. The theoretical curves are prepared with the modified Jankus theory for an exponential model of the neutron's magnetic moment density and various choices of rms radius shown in the figure. The proton radii are taken to be $0.80\times10^{-13}$ cm. A neutron radius of $0.90\times10^{-13}$ cm fits the experimental data fairly well.

When the experiments are carried out[6,29] at 500 Mev and at 600 Mev, the two sets of data in Figs. 28 and 29 and Table II are obtained. Various theoretical curves for an exponential model of a neutron with sizes 0.60, 0.61, 0.80, and $1.0\times10^{-13}$ cm are also shown in these figures. The rms size $0.85\times10^{-13}$ cm for an exponential model fits all the experiments fairly well. Calculations with other models of a neutron are in progress, but it seems clear that the rms size cannot differ very much from $r_m{}^N=0.80\times10^{-13}$ cm. Thus it appears the neutron and proton have magnetic sizes and structures that are the same within present experimental error! The error in the size determination is probably of the order of, or less than, $0.15\times10^{-13}$ cm.

TABLE II. Differential (peak) cross sections for the deuteron at 500 and 600 Mev at various scattering angles.

| 500 Mev | | 600 Mev | |
|---|---|---|---|
| $\theta$ | $d^2\sigma_D/d\Omega dE$ (cm$^2$/sterad Mev) | $\theta$ | $d^2\sigma_D/d\Omega dE$ (cm$^2$/sterad Mev) |
| 45° | ... | 45° | $(5.30\pm0.52)\times10^{-33}$ |
| 60° | ... | 60° | $(1.32\pm0.13)\times10^{-33}$ |
| 75° | $(8.60\pm0.52)\times10^{-34}$ | 75° | $(6.35\pm0.65)\times10^{-34}$ |
| 90° | $(3.85\pm0.57)\times10^{-34}$ | 90° | $(1.96\pm0.44)\times10^{-34}$ |
| 105° | $(2.96\pm0.52)\times10^{-34}$ | 105° | $(1.54\pm0.52)\times10^{-34}$ |
| 120° | $(2.00\pm0.30)\times10^{-34}$ | 120° | $(9.38\pm2.78)\times10^{-35}$ |
| 135° | $(1.51\pm0.22)\times10^{-34}$ | 135° | $(8.0\ \pm0.70)\times10^{-35}$ and $(6.0\ \pm0.91)\times10^{-35}$ |

These results suggest that the area method may best be used to investigate the small effects of the various corrections we have mentioned in discussing that method.

The possibility that the neutron's charge cloud ($F_{1N}\neq0$) may have relatively large excursions as a function of radius has been considered by Schiff,[38] who uses the area method to evaluate the neutron form factors. He concludes that it is most likely that the neutron charge density is zero.

## III. REMARKS ON THE SIGNIFICANCE OF THE RESULTS

This general problem has already been dealt with in an excellent article by Yennie *et al.*[8] summarizing the information as of a year and one-half ago. Since the innermost parts of the neutron and proton cannot be known at the present stage of our knowledge in physics, the correct experimental observations of structure can be taken as primary facts of nature. In this event, there are, of course, no anomalies. However, it is the aim of theory to attempt to fit the unknown into what is already known, and the proton and neutron structures are no exceptions to this aim. In the known (or rather, partially known) category of physical theory, we include the present body of meson field theory. Perhaps, with respect to this body of knowledge, an "anomaly" may be said to exist: That is, the *proton's* Dirac cloud

[38] L. I. Schiff, Revs. Modern Phys. **30**, 462 (1958), this issue.

(governed by $F_1$) appears to be very different from the neutron's corresponding cloud. This is a difficulty which has existed for some time in the interpretation of the neutron-electron experiments[18–22,39] on the basis of meson theory. The fact that the second radial moment of the charge distribution is almost exactly zero makes "it seem unlikely that any theory which describes only the pion charge cloud associated with the neutron, ignoring spatial distribution of the charge on the residual neutron core, will predict a vanishing $r^2$ moment," as Salzman has remarked.[40] The new experiments reported here do not enhance the nature of this difficulty, but, on the contrary, reinforce the view that the outer or pionic clouds of neutron and proton are basically similar, if one may judge these by the magnetic moment distributions. It is possible that small differences, not detectable in the present experiments, may yet exist in the outer (pionic) regions.

Perhaps there are also relatively large differences in the innermost parts of these two nucleons. Only experiments at higher energies (0.5 to 1.5 Bev) or more precise experiments at the present energies can furnish the answers to such problems.

Using the Chew-Low theory[41] and an upper cutoff momentum, Salzman[40] succeeded in showing that the electron-proton scattering data[7–10] at energies up to 236 Mev could be satisfactorily explained with a spread-out core distribution. The spread-out core is consistent with Salzman's earlier explanation of the anomalous neutron-electron results,[42] but the use of such a large core is not readily understandable in terms of the expected (smaller) dimensions associated with nucleons, antinucleons, or heavy mesons of various kinds. Attempts in this direction have been made by Sandri[43] and Tamm.[44]

Recently, dispersion-theoretic attacks have been made on the nucleon structure problem by a number of authors.[45–47] Chew *et al.* point out that[45] the magnetic moment "size" can be explained by the two-pion state, but that higher mass-configurations may be responsible for the charge "size." We do not know whether the assumptions involved in this treatment are equivalent to the large core hypothesis of Salzman, but it is apparent, once more, that to resolve the present problems, new data at higher energies, corresponding to the probing of smaller dimensions, are needed. Whether electrodynamics is valid in the realm of these same small dimensions is the dominant question. The presence of difficulties in our understanding of nucleon structure may be a forerunner of the troubles to be expected at very small distances when dealing with quantum electrodynamics[48,49] or with our concepts of space and time. It is also not clear why $F_1 \cong F_2$ as appears to be true in the case of the proton. This is another problem to be added to those already posed.

## ACKNOWLEDGMENTS

We thank Mr. R. Blankenbecler for many stimulating discussions on the theory of electrodisintegration of the deuteron. We also thank Professor S. Drell for illuminating comments and helpful remarks on our work and, in particular, for his suggestion to emphasize the "peak" method of determining neutron size. Dr. W. Schneider and Dr. V. Z. Jankus have also aided us with their calculations on the deuteron. Conversations with Professor G. Chew, Professor M. Goldberger, Professor R. Karplus, and Professor F. Zachariasen have been helpful and encouraging. We also thank Professor L. I. Schiff for permitting us to examine his results before publication. We express appreciation to Mr. G. R. Burleson, Mr. C. N. Davey, Dr. H. W. Kendall, and Mr. G. Gilbert and the accelerator crew for their valuable assistance in obtaining the experimental data. We appreciate the constructive comments of Mr. S. Sobottka.

[39] R. Sachs and S. Treiman, Phys. Rev. **103**, 435 (1936).
[40] G. Salzman, Phys. Rev. **105**, 1076 (1957).
[41] G. F. Chew and F. E. Low, Phys. Rev. **101**, 1570 (1956); **101**, 1579 (1956).
[42] G. Salzman, Phys. Rev. **99**, 973 (1955).
[43] G. Sandri, Phys. Rev. **101**, 1616 (1956).
[44] I. Tamm, reported in footnote 38 of reference 8.
[45] Chew, Karplus, Gasiorowicz, and Zachariasen (to be published).
[46] J. Bernstein and M. L. Goldberger, Revs. Modern Phys. **30** 465 (1958), this issue.
[47] K. Tanaka (to be published).
[48] R. P. Feynman, Anais acad. brasil. cienc. **26**, (1954) (in English).
[49] S. Drell, Bull. Am. Phys. Soc. Ser. II, **2**, 376(T) (1957).